Ocean Modelling 65 (2013) 11–24

Contents lists available at SciVerse ScienceDirect

Ocean Modelling

journal homepage: www.elsevier.com/locate/ocemod

Assessing the impact of downscaled winds on a regional ocean model simulation of the Humboldt system

Gildas Cambon [a,*], Katerina Goubanova [a,b,c], Patrick Marchesiello [a], Boris Dewitte [a,b], Séréna Illig [a,c], Vincent Echevin [d]

[a] Laboratoire d'Études en Géophysique et Océanographie Spatiale, UMR 5566, IRD/CNRS/CNES/UPS, 14, Avenue Edouard Belin, 31400 Toulouse, France
[b] Instituto Geofísico del Perú, Lima, Peru
[c] Instituto del Mar de Perú, Callao, Peru
[d] Laboratoire d'Océanographie et de Climatologie: Expérimentation et Analyse Numérique, UMR 7159, IRD/CNRS/UPMC/MNHN, Paris, France

ARTICLE INFO

Article history:
Received 7 August 2012
Received in revised form 29 November 2012
Accepted 25 January 2013
Available online 16 February 2013

Keywords:
Regional modeling
Atmospheric forcing
Statistical downscaling
Peru–Chile upwelling system
El Niño

ABSTRACT

Simulating the oceanic circulation in Eastern Boundary Upwelling Systems (EBUS) is a challenging issue due to the paucity of wind stress products of a sufficiently high spatial resolution to simulate the observed upwelling dynamics. In this study, we present the results of regional simulations of the Humboldt current system (Peru and Chile coasts) to assess the value of a statistical downscaling model of surface forcing. Twin experiments that differ only from the momentum flux forcing are carried out over the 1992–2000 period that encompasses the major 1997/98 El Niño/La Niña event. It is shown that the mean biases of the oceanic circulation can be drastically reduced simply substituting the mean wind field of NCEP reanalysis by a higher resolution mean product (QuikSCAT). The statistical downscaling model improves further the simulations allowing more realistic intraseasonal and interannual coastal undercurrent variability, which is notoriously strong off Central Peru and Central Chile. Despite some limitations, our results suggest that the statistical approach may be useful to regional oceanic studies of present and future climates.

1. Introduction

The Humboldt current system (HCS) also known as the Peru Chile current system is the Eastern Boundary Upwelling System (EBUS) of the South Pacific Ocean. The coastal ocean off Chile and Peru is characterized by the upwelling of cold, nutrient-rich waters driving an exceptionally high biological productivity (Carr and Kearns, 2003) and making this system the most productive marine ecosystem in the world (Chavez et al., 2008). The HCS upwelling is driven by persistent equatorward, upwelling-favorable winds that have a marked seasonal cycle and intraseasonal variability. Two main upwelling regions can be considered: Central Chile and Central Peru regions. The former is characterized by seasonally varying wind-forced upwelling with a peak season in Austral Summer that is modulated by atmospheric coastal jets (Garreaud and Muñoz, 2005). Coastal jets are intermittent upwelling favorable winds driven by the extra-tropical storm activity entering the region of the South–East Pacific (SEP) anticyclone (Renault et al., 2009). The Central Peru region (∼15°S) is comparable to the Central Chile region except that the seasonal cycle of the upwelling has weaker amplitude and peaks in Austral winter. This region is also under the influence of intermittent/intraseasonal upwelling favorable winds that share many characteristics with Central Chile coastal jets (Dewitte et al., 2011).

Many features of the oceanic circulation in the Humboldt system are critically dependent on the characteristics of coastal winds. Coastal winds and wind-stress curl drive upwelling velocities and alongshore transports, which determine the vertical temperature structure of the coastal area (Capet et al., 2004; Estrade et al., 2008; Marchesiello et al., 2010; Renault et al., 2012). Furthermore, intense mesoscale activity (compared to the mean currents) results from baroclinic instability of the wind-driven coastal currents (Marchesiello et al., 2003) and feeds back to the tracer properties and biological productivity (Gruber et al., 2011).

A realistic simulation of the regional circulation in the Humboldt system and in EBUS in general requires that the main features of regional circulation (upwelling rate, alongshore circulation and mesoscale activity) be simulated with a certain degree of realism. To that end, satellite wind forcing has proven valuable in the Northern Humboldt system at seasonal timescales (Penven et al., 2005; Montes et al., 2010, 2011; Albert et al., 2010; Echevin et al., 2011; Colas et al. 2011; Aguirre et al., 2012) and during the 1997/98 El Niño event (Colas et al., 2008). However, these studies have highlighted the limitations associated with

* Corresponding author. Tel.: +33 5 61 33 28 37; fax: +33 5 61 25 32 05.
E-mail address: gildas.cambon@legos.obs-mip.fr (G. Cambon).

1463-5003/$ - see front matter © 2013 Elsevier Ltd. All rights reserved.
http://dx.doi.org/10.1016/j.ocemod.2013.01.007

relatively short records of observed wind products (less than 10 years for both the ERS and QuikSCAT data sets), which prevents addressing longer timescales of variability including the climate change problem.

To access long-term atmospheric forcing, global model reanalyzes or climate simulations are needed. However, their coarse resolution (typically ~2–3°) does not allow an adequate representation of regional dynamical processes, such as the influence of the Andes Mountains on the atmospheric circulation, or local processes driven by small-scale land–ocean–atmosphere interaction.

To circumvent this resolution issue, dynamical or statistical downscaling methods can be used to represent key features at the appropriate spatial scales. Whereas dynamical downscaling is, in general, cumbersome due to computational costs associated with the use of high-resolution mesoscale atmospheric models, statistical downscaling offers a cost effective alternative. In the Peru–Chile coastal ocean, Goubanova et al. (2011) showed that statistical downscaling of reanalysis products provide improved coastal winds over extensive time periods. They call for assessing to which extent this improvement can be valuable for long-term oceanic regional simulations. This is the objective of the present study that can be viewed as an oceanographic extension of Goubanova et al. (2011).

The study focuses on the 1992–2000 period that experiences strong interannual variability associated with the 1997/98 El Niño and benefits from the availability of independent wind observations from those used in the statistical model. A series of numerical experiments are performed using different wind products including NCEP/NCAR atmospheric reanalysis. Key features of the regional circulation off Peru and Chile are considered in order to evaluate the benefit in using downscaled atmospheric products for high-resolution oceanic modeling studies. The focus is on the impact of the wind stress forcing onto both the mean coastal circulation and its intraseasonal and interannual fluctuations. The vertical structure variability of the along-shore oceanic coastal current is particularly relevant to the dynamics of the HCS as it favors mesoscale activity (Strub et al., 1998; Penven et al., 2005) and influences the oceanic teleconnexion with the equatorial region (Pizarro et al., 2002). Its representation in ocean models is therefore a key element to ensure some realism of a variety of processes. It will be used here as a benchmark to evaluate the impact of the wind stress products over the two regions of peak variability, i.e., Central Peru and Central Chile.

The paper is organized as follows. In the next section, the data and ocean model are presented along with a brief description of the statistical downscaling method of atmospheric forcing. In Section 3 we evaluate the impact of the applied atmospheric downscaling on the oceanic response, firstly assessing the realism of the mean and surface eddy circulation, then the intraseasonal and interannual variability of subsurface currents. Finally, a summary and some concluding remarks of this work are presented in Section 4.

2. Data and methods

2.1. Wind stress data forcing

2.1.1. ERS satellite winds

Our control run is forced by the ERS scatterometer wind stress provided by CERSAT (http://www.ifremer.fr/cersat; Bentamy et al., 1996; CERSAT, 2002a). The ERS product is derived from weekly averaged 50 km resolution ERS 1–2 swath data (swath width is 500-km) and spatially interpolated by a kriging method. It covered the global ocean in 3 days and operated from January 1991 to December 2000. A weekly product is available from January 1992 to December 2000, which sets our study period.

2.1.2. NCEP2 wind stress

The NCEP Reanalysis II (NCEP2) data is a joint product from the National Centers for Environmental Prediction and the National Center for Atmospheric Research (Kanamitsu et al., 2002). This product or its earlier version (NCEP1) has been used in very few EBUS model studies (Rouault et al., 2009) because of its low resolution of 2.5° × 2.5°. It will be used here to both force a reference oceanic solution and build the downscaled wind forcing that provides our new solution. It will appear that the original NCEP2 wind product leads to severe biases of the simulated mean circulation of the Humboldt system and its variability.

2.1.3. Statistically downscaled wind stress

Goubanova et al. (2011) recently developed a statistical downscaling method for assessing the impact of climate change on the atmospheric circulation along the coasts of Peru from a low-resolution coupled model. The model is based on a multiple linear regression between local/regional variables (predictand) and large-scale climate characteristics (predictors) in the present-day climate. The predictand is the near-surface wind measured by QuikSCAT scatterometer (gridded product from CERSAT, 2002b: 0.5° × 0.5° spatial resolution, 1-day temporal resolution from 2000 to 2008, with a 25 km blind zone near the coast). This product is assumed to offer the best quality long-term daily time series. The large-scale predictors, covering the QuikSCAT period, are the sea level pressure (SLP) and near-surface wind fields from NCEP2 reanalysis data. The statistical relations between predictand and predictors were then used to downscale NCEP2 surface winds for the period 1979–2001 (NCEP1 was also downscaled for the period 1958–2001 but not used in this study). The statistical model is applied on wind anomalies relative to a reference mean seasonal cycle that is taken from QuikSCAT data. This technique allows an important correction of coastal jet patterns off Central Peru and Central Chile due to QuikSCAT accuracy (Garreaud and Munoz, 2005; Dewitte et al., 2011). In the NCEP product, coastal jets are located too far offshore leading to patterns of coastal wind curl that favor Ekman pumping rather than coastal upwelling (Colas et al., 2011) and impact alongshore transport (Marchesiello et al., 2003). In addition, low-frequency variability and long-term trends present in NCEP2 reanalysis are preserved assuming that the downscaling approach keeps a share of the regional winds decadal variability. This leads to a low-frequency modulation of the mean seasonal signal in the downscaled product. Consequently, the latter presents weaker mean coastal winds for the period 1992–2000 than the QuikSCAT product (Fig. 1(c) and (d)). At interannual scales, the downscaling of wind anomalies captures some of the El Niño-La Niña features, namely the increase (decrease) of along-shore wind stress off Central Peru (Chile) during El Niño and the El Niño-La Niña asymmetry, whereas at synoptic and intraseasonal scales, it reproduces most of the along-shore wind stress variability originating from subtropical storms activity. Namely the decrease (increase) of along-shore wind stress off Central Peru (Chile) during El Niño and the El Niño–La Niña asymmetry. Finally at intraseasonal scales, the downscaled product captures some of the synoptic along-shore wind stress variability originating from subtropical storm activity. The reader is referred to Goubanova et al. (2011) for more details on the method and its skills in simulating the regional atmospheric circulation off Peru and Chile.

2.2. Experimental design

A series of modeling experiments were conducted that differs only by the wind forcing as summarized in Table 1. The control run (R-ERS) uses ERS winds and is a benchmark for the evaluation of all other experiments. We choose R-ERS as a benchmark because it is the only simulation using observed wind for the studied period; some validation results are presented in the next Section 2.3. R-NCEP2_DS is the experiment with NCEP2 downscaled winds at a daily resolution. Two other experiments use NCEP2 winds, either the raw NCEP2 product (R-NCEP2) or a variant where the mean seasonal cycle is replaced by QuikSCAT climatology (R-NCEP2_QSCLM). With the first one will be assessed the overall improvement of the downscaled product; the second experiment will help assess the benefit of downscaling wind anomalies in addition to the mean structure. Finally, a climatological run is considered, where ROMS is forced with QuikSCAT climatological winds (R-QSCLM). This simulation will provide a reference for assessing non-locally forced oceanic variability, i.e. intrinsic variability from instabilities of the mean currents and forced variability by oceanic boundaries (in particular of equatorial origin). An additional experiment, called R-NCEP2_DS_7D is designed to test the impact of synoptic wind forcing on the intraseasonal variability, and consists of averaging NCEP2_DS over 7-days bins. This latter experiment will allow a direct comparison with R-ERS, which also uses wind stress forcing at a 7-day resolution.

2.3. Data set description

2.3.1. Reynolds sea surface temperature

We used the 0.25° resolution Reynolds SST (Reynolds et al., 2007) from NCDC (http://www.ncdc.noaa.gov), over the period 1992–2000 to verify the model mean SST.

2.3.2. SSALTO/DUACS altimetry data

Observed sea level anomaly (SLA) is used for model evaluation of the surface eddy circulation. The DUACS (Ducet et al., 2000) gridded product is supplied by AVISO (CLS, Toulouse, France) from 14 October 1992 to 27 December 2001, with a nominal resolution of 1/3° every week. These measurements are obtained from merged TOPEX POSEIDON, ERS and Jason gridded data. To estimate mesoscale activity, surface geostrophic eddy kinetic energy (EKE) is computed using geostrophic velocities derived from SLA. The same method is used to compute both satellite and model EKE and it was checked that the ageostrophic component of EKE remains weak, as in the California current system study of Marchesiello et al. (2003).

2.3.3. Tide gauge data

Tide gauge data are used as independent observations to evaluate the skills of the regional model. The data from nine stations along the Peruvian and Chilean coasts from Talara (4.58°S) to Valparaiso (33.03°S) were available and provided by The University of Hawaii Sea Level Center at (http://ilikai.soest.hawaii.edu/uhslc/data.html). Tides provided by GOT4.7 (Ray, 1999) were removed from the data, as well as the high frequency response to atmospheric forcing (wind and pressure) using the Dynamic Atmospheric Correction (DAC). The latter is based on a global barotropic model (Mog2D; Carrère and Lyard, 2003) for high frequency correction (i.e., less than 20 days) and an Inverted Barometer correction for lower frequency. The data are then monthly-averaged and detrended before calculating the interannual sea-level anomalies (SLA). The resulting time series are used to validate the model coastal sea level through Taylor's skill score (Taylor, 2001): $S = 2\,(1+R)/(\hat{\sigma}+1/\hat{\sigma})^2$, which measures the combined cost of poor correlation (R) and standard deviation errors ($\hat{\sigma}$ is the ratio of standard deviation between model and data). Correlation and skill score at the nine tide gauge locations and for all simulations are discussed in Section 3.

2.4. Ocean model setup

The numerical model used in this study is ROMS (Shchepetkin and McWilliams, 2005), in its version with 2-way nesting capability (ROMS_AGRIF, Penven et al., 2006; Debreu et al., 2012). ROMS is a split explicit, free-surface, topography-following coordinate model that solves the primitive equations based on the Boussinesq and hydrostatic approximations. It uses mixed active–passive open boundary conditions (Marchesiello et al., 2001), the KPP boundary layer scheme (Large et al., 1994) for vertical turbulent closure and a rotated lateral hyperdiffusion operator to avoid excessive diapycnal mixing (Marchesiello et al., 2009).

The model grid, forcing, and initial conditions are built using the ROMSTOOLS package (Penven et al., 2008). The configuration is similar to the one used in Echevin et al. (2012) and Belmadani et al. (2012). The domain extends from 15°N to 40°S, and from the coast to 100°W, with three lateral open boundaries at the south, north, and west. The horizontal grid resolution of ~1/6° (exactly at the equator) was selected as a trade off between the need to resolve fundamental mesoscale eddy features and the computational cost of a large domain size and numerous sensitivity experiments. Since the wavelength associated with the first baroclinic Rossby radius along the coast of the study region varies from ~600 km near the equator to ~200 km at 35°S (Tulloch et al., 2011), mesoscale eddies would be well resolved at 1/6° resolution, especially off Peru. However, in upwelling systems, lateral buoyancy gradients are largely dependent on upwelling intensity and thereby on the scale of coastal Ekman divergence, which roughly equals 5 km off both Peru and Chile (Estrade et al., 2008; Marchesiello and Estrade, 2010). A coarse resolution of coastal Ekman divergence would thus affect upwelling intensity and lower the source of available potential energy used by baroclinic instability to produce eddies. This limitation is common to all recent regional studies of the Peru–Chile region (Colas et al., 2011; Renault et al., 2012) and needs to be better assessed using a critical approach of observational estimates (see Swenson and Niiler, 1996). This is beyond the scope of the present work and for our purposes the good representation within uncertainties of mesoscale activity will suffice (see comparison of surface EKE maps in Section 3 and further discussion in Belmadani et al., 2012).

The vertical grid has 32 levels stretched to increase vertical resolution near the surface. Following (Penven et al., 2005), bottom topography, h, from ETOPO2 (Smith and Sandwell, 1997) was interpolated on the model grid and smoothed in order to keep a "slope parameter" $r = \frac{\nabla h}{h} < 0.2$ (Beckmann and Haidvogel, 1993), to reduce pressure gradient errors. The model is forced by fresh water and heat fluxes extracted from the Comprehensive Ocean–Atmosphere Data Set (COADS) ocean surface monthly climatology at 1/2° resolution (Da Silva et al., 1994). This dataset is also used to restore model SST and sea surface salinity to climatological value through a heat-flux correction (Barnier et al., 1995). The boundary forcing is provided by 5-day mean oceanic outputs from the SODA 2.3.4 Reanalysis (Carton and Giese, 2008) for temperature, salinity, horizontal velocity and sea level over the period 1992–2000. SODA assimilates observational data in a general circulation model based on the Parallel Ocean Program (Smith et al., 1992), with an average horizontal resolution of 0.25° × 0.4° in latitude–longitude and 40 vertical levels with 10-m spacing near the surface. The reader is referred to Carton and Giese (2008) for a detailed description. Note that this 5-day mean dataset provide a realistic forcing of the intraseasonal Kelvin wave (Dewitte et al., 2008) which is influential on the upwelling variability off Central Peru and Central Chile (Hormazabal et al., 2001, 2002; Dewitte et al., 2011). This will provide a relevant comparison of the various simulations for intraseasonal variability along the coast. Initial conditions are also derived from the SODA reanalysis on the 1st of January 1992. The forcing, initial and boundary conditions were linearly interpolated on ROMS grid using ROMSTOOLS over the period 1992–2000. A 3-year spin-up using a repeated forcing of the year 1992 was sufficient to reach a statistical equilibrium.

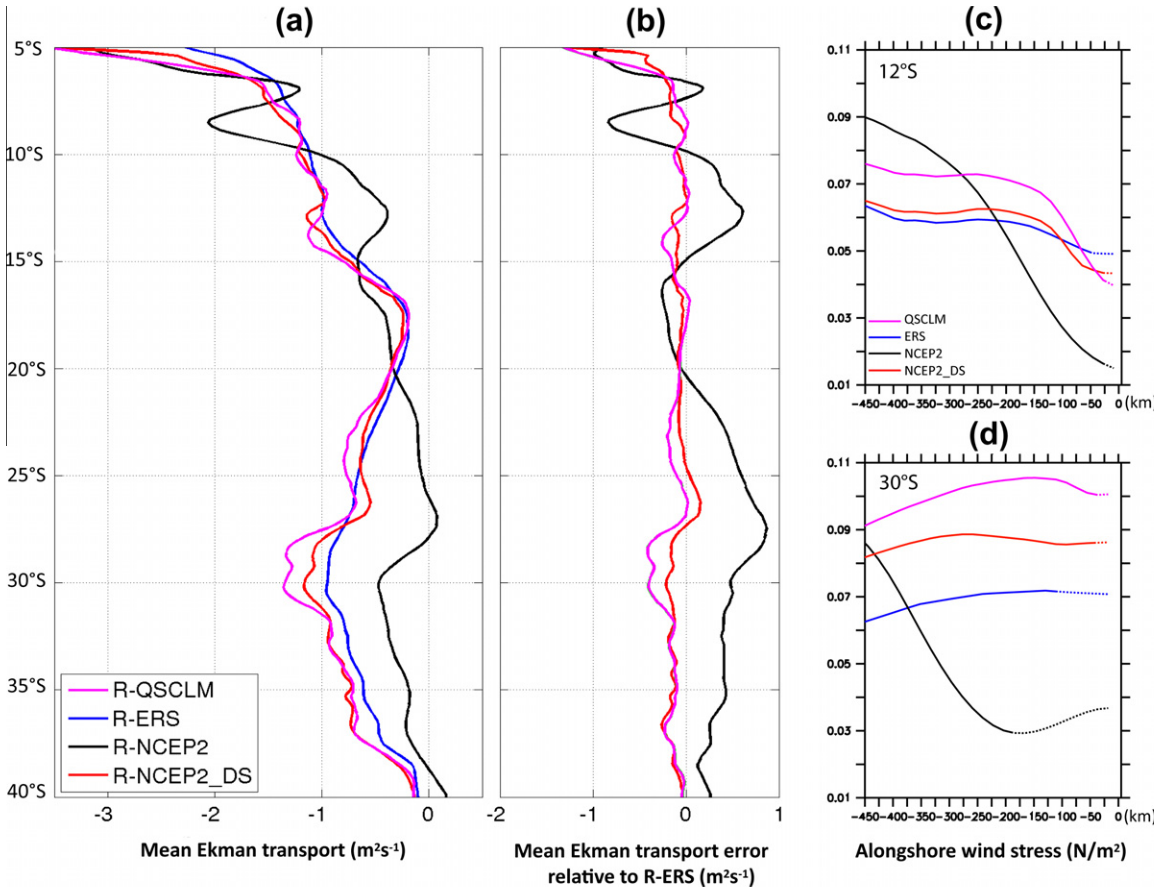

Fig. 1. Ekman transport over the period 1992–2000 (in $m^2\ s^{-1}$) as a function of latitude, and as derived from the different wind stress forcing presented in Table 1: (a) Mean seasonal Ekman transport, (b) Differences relative to the ERS control wind stress forcing. The Ekman transport is computed from the along-shore wind stress, obtained by projecting the meridional and zonal components along the coastline direction as derived from ETOPO (1° resolution) using 3°-wide segments. The values are smoothed using a running mean of 10 grid points to filter noisy patterns, (c) Cross-shore profiles of alongshore wind stress (in N/m^2) at 12°S and (d) at 30°S. The dashed lines indicate the blind zone region of wind products where ROMS wind forcing is extrapolated from offshore values.

Table 1
Summary of experiments.

Simulation name	Wind stress forcing	Spatial and temporal resolution of gridded wind product	Main objectives
R-ERS	ERS	Weekly forcing and 50-km spatial resolution	Validation (control run)
R-NCEP2	NCEP2	6-hourly forcing and 2.5° × 2.5°spatial resolution.	Assessing the benefit of downscaling NCEP2
R-NCEP2_DS	NCEP2_DS	Daily forcing and 0.5° × 0.5°spatial resolution	Assessing the benefit of downscaling NCEP2
R-NCEP2_DS_7D	NCEP2_DS_7D	Weekly forcing and 0.5° × 0.5° spatial resolution	Assessing the impact of synoptic-scale forcing
R-NCEP2_QSCLM	QuikSCAT climatology (2000–2008) + NCEP2 anomaly: NCEP2_QSCLM	Monthly QuikSCAT climatology and NCEP2 daily anomalies. Spatial resolution is 0.5° for QuikSCAT and 2.5° × 2.5° for NCEP2.	Assessing the benefit of downscaling NCEP2 compared with simply replacing its mean seasonal state with QuikSCAT climatology
R-QSCLM	QuikSCAT climatology (2000–2008): QSCLM	Monthly climatology and 0.5° × 0.5° spatial resolution	Assessing the role of local interannual and non-seasonal forcing

3. Results

3.1. Ekman dynamics

In the next section, we will consider the mean ocean response to the various wind products, i.e., SST, circulation and EKE patterns. In upwelling regions, these features are highly sensitive to the characteristics of both the mean along-shore wind stress amplitude and coastal wind stress curl. In the Humboldt system, sustained equatorward alongshore winds produce offshore Ekman transport and negative wind stress curl that results in both coastal upwelling and Ekman pumping respectively (Halpern, 2002; Croquette et al., 2007). The main driver of the tridimensional coastal circulation is coastal upwelling (Capet et al., 2004) which is related to the alongshore wind stress τ_a by the offshore Ekman transport $\tau_a/f\rho_0$ (f is Coriolis frequency and ρ_0 density of sea water). It is thus of interest, as a preliminary comparison, to investigate the direct and linear ocean response to wind stress.

Fig. 1(a) presents the 1992–2000 mean Ekman transport along the whole west coast of southern America and for the various wind products of Table 1. The comparison confirms that NCEP2 leads to the weakest mean Ekman transport. This is largely due to the overestimation of coastal wind drop-off in the reanalysis resulting from Gibbs phenomenon and low-order spectral representation of the

Table 2
Spatial pattern correlations of 1992–2000 mean surface EKE between model solutions and AVISO observations over the "Chilean Box". In these calculations, we only consider EKE values greater than 80 cm^2/s^2 for total-EKE and 20 cm^2/s^2 for intraseasonal-EKE.

Simulations	EKE spatial pattern correlations "Chilean Box": [24–36°S]–[Coast–85°W]	
	Intraseasonal-EKE	Total-EKE
R-ERS	0.84	0.75
R-NCEP2	0.73	0.60
R-NCEP2_QSCLM	0.86	0.68
R-NCEP2_DS	0.88	0.77
R-QSCLM	0.83	0.74

steep coastal range and Andean mountains (Kanamitsu et al., 2002; Renault et al., 2012). The satellite products show closer Ekman transports than NCEP2 (NCEP2_QSCLM shares the same mean wind stress as QSCLM by construction and is thus not shown). There is a relative good agreement between ERS and QuikSCAT-based products (as in Croquette et al., 2007) but with differences. Some of the differences can be attributed to the different periods of satellite measurement (1992–2000 for ERS; 2000–2008 for QuikSCAT). Therefore, the fact that NCEP2_DS is generally closer to ERS than QSCLM is a positive result that can be attributed to the downscaling of low-frequency variability in NCEP2_DS. However, some ERS biases were previously noticed by Blanco et al. (2001) for a limited area around 23°S and related to the larger blind zone of ERS compared with QuikSCAT. As a result of a larger blind zone and coarser resolution, the wind stress curl of ERS (Fig. 1(c) and (d)) is 2–3 times lower than QuickSCAT in the 100-km wide coastal region affected by SST-wind interactions (Chelton et al., 2007). Interestingly, the downscaled product appears to retain some of QuikSCAT skills in representing this coastal wind profile, which is best evidenced in the Central Peru region (Fig. 1(c)).

3.2. Mean ocean response

In situ hydrographic measurements are relatively sparse in the Southeast Pacific. The simulated SST is assessed against the Reynolds climatology. The observed and modeled mean SST fields are presented in Fig. 2. The general agreement in the offshore region is not surprising considering that the model surface heat forcing contains a nudging term to climatological SST (Barnier et al., 1995). However, a clear bias is apparent near the coast in R-NCEP2 due to the noted weakness of its coastal winds forcing and associated coastal upwelling response. This bias is significantly reduced in the simulations using QuikSCAT seasonal winds. Similar conclusions can be drawn from comparisons with climatological mixed layer depth derived from CARS2009 data (Ridgway et al., 2002; not shown).

The 3D response to wind stress forcing can be partly understood from Ekman and Sverdrup dynamics. The vertical structure of alongshore currents is particularly interesting as it is largely dependent on the mean coastal wind forcing and is known to control the production of regional mesoscale turbulence (Marchesiello et al., 2003). Fig. 3 presents meridional current sections off Central Peru for all model experiments. It can be compared to other modeling studies of this region (e.g. Penven et al., 2005; Montes et al., 2010; Colas et al., 2011). The circulation is characterized by an intense northward coastal current of ~12 cm/s (Peru Coastal current, hereafter PCC) flowing over a southward undercurrent (Peru–Chile Undercurrent, hereafter PCUC) that is attached to the slope and peaks around 150 m (Montes et al., 2010). Not surprisingly R-NCEP2 fails to realistically simulate these features (Fig. 3(b)) because of underestimated coastal wind and overestimated wind curl. As a result, the surface coastal current is too weak and the undercurrent peaks offshore near the surface (consistently with Sverdrup balance between wind stress curl and meridional transport). The other simulations exhibit closer vertical current structure to the literature's standard. This can be attributed to their more accurate mean forcing derived from scatterometer measurement. R-NCEP2_QSCLM shows similar results to R-ERS, R-QSCLM and R-NCEP2_DS even though only the mean seasonal cycle has been changed from the original NCEP2 product. The similarity is particularly striking when comparing with R-QSCLM, which shares exactly the same mean seasonal forcing. This result confirms that the mean circulation in upwelling current systems is largely driven by the mean seasonal wind forcing (Marchesiello et al., 2003). Interestingly though, R-NCEP2_DS is closer to R-ERS than R-QSCLM or R-NCEP2_QSCLM. Both R-NCEP2_DS and R-ERS show a weaker PCUC and stronger surface coastal current, which could be attributed to residual effects of interannual wind events in the low-frequency spectrum. In particular, during the 1997/98 El Niño, there is a increase of the along-shore wind stress off Central Peru (Goubanova et al., 2011) that may participate in weakening the PCUC (see Section 3.3) despite increased stratification. The maintenance of trends and low-frequency variability in NCEP2_DS is thus of importance.

Fig. 4 is similar to Fig. 3 but for the Central Chile region where a comparable vertical along-shore current structure can be found. It can also be compared to other modeling studies (Colas et al., 2011; Aguirre et al. 2012). The PCUC core is deeper than that off Peru, located around 250 m with a deeper vertical extension reaching more than 400 m depth. The maximum speed of 20 cm/s at 30°S (in R-ERS) is comparable to the observational value of 13 cm/s given in Shaffer et al. (1999) or to other model estimates (Aguirre

Table 3
Comparison of interannual sea level anomalies between continuous observations at 9 tide gauge stations along the coasts of Peru and Chile and the model solutions for R-ERS, R-NCEP2, R-NCEP2_QSCLM and R-NCEP2_DS experiments. The tidal signal was removed from the gauge data (Ray, 1999). S is the model skill score defined by Taylor (2001) that measures the combined cost of poor correlation and standard deviation errors: $S = 2\,(1+R)/(\hat{\sigma}+1/\hat{\sigma})^2$, where $\hat{\sigma}$ is the ratio of standard deviations between model solution and data (maximum is 1) and R is their relative correlation. Bold values are for maximum correlations and scores.

Station	Latitude	R-ERS		R-NCEP2		R-NCEP2_QSCLM		R-NCEP2_DS	
		R	S	R	S	R	S	R	S
Talara	4.58°S	0.62	0.72	0.62	0.70	**0.63**	**0.75**	0.62	**0.75**
Paita	5.08°S	0.72	0.86	0.71	0.85	0.72	0.86	**0.75**	**0.87**
Callao	12.02°S	0.87	0.88	0.86	0.89	0.88	0.9	**0.90**	0.93
Pisco	13.72°S	0.69	0.65	0.75	0.75	0.73	0.70	**0.78**	**0.76**
San Juan	15.36°S	0.69	0.79	0.75	0.85	**0.77**	0.85	0.76	**0.86**
Matarani	17.05°S	0.74	0.83	**0.79**	**0.89**	0.78	0.87	0.78	0.88
Antofagasta	23.65°S	0.45	0.65	**0.55**	**0.72**	0.54	0.71	0.48	0.71
Caldera	27.06°S	**0.70**	0.72	0.64	0.69	0.65	0.72	0.69	0.77
Valparaiso	33.03°S	0.76	0.62	0.75	0.67	0.77	0.61	**0.82**	**0.71**

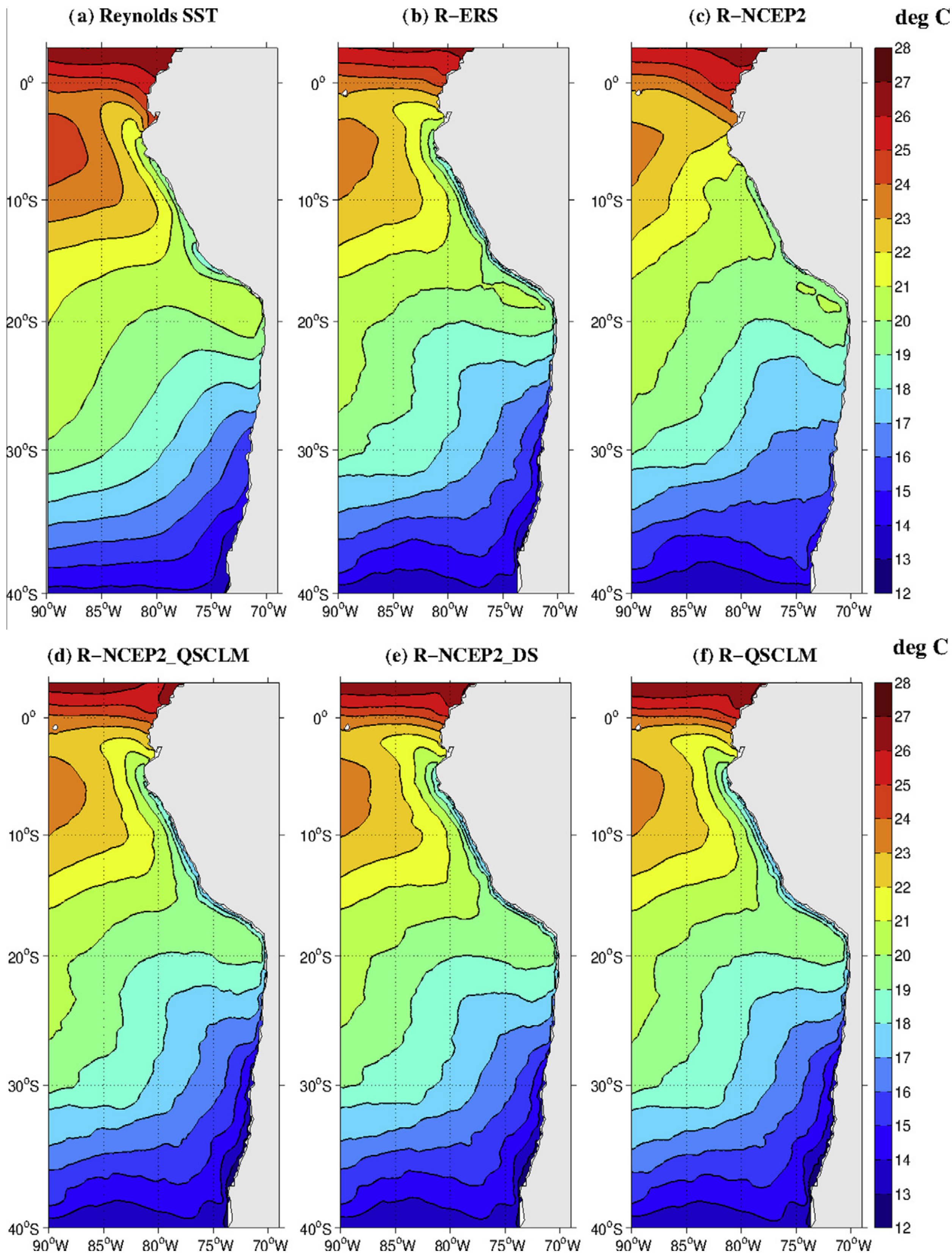

Fig. 2. Mean sea surface temperature over the period 1992–2000 for (a) Reynolds SST observations and the various simulations: (b) R-ERS, (c) R-NCEP2, (d) R-NCEP2_QSCLM, (e) R-NCEP2_DS and (f) R-QSCLM.

et al., 2012). Finally, as previously noticed in Colas et al. (2011), the PCUC tends to outcrop right outside the equatorward coastal current around 100 km offshore. Again, a large difference appears between R-NCEP2 and the other simulations, which reflects the large bias in the NCEP2 wind pattern. As in the Central Peru region, R-NCEP2_DS compares better to R-ERS than the QSCLM-based

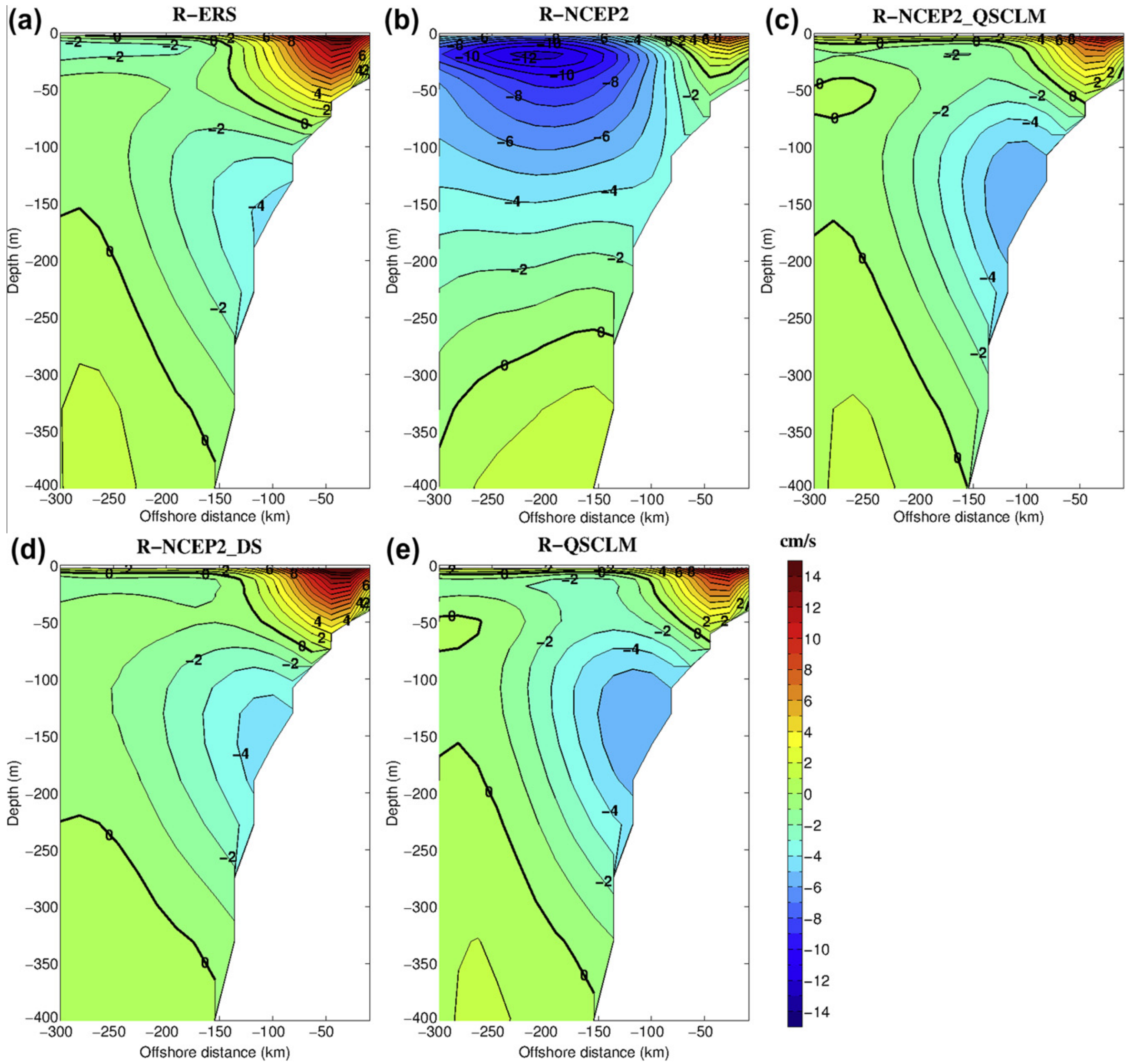

Fig. 3. Vertical sections of mean meridional current (in cm.s^{-1}) off Central Peru (alongshore-averaged between 7°S and 13°S) for the various simulations: (a) R-ERS, (b) RNCEP2, (c) R-NCEP2_QSCLM, (d) R-NCEP2_DS and (e) R-QSCLM. Contour interval is 1 cm.s^{-1}.

simulations, but there is a lesser impact of low frequency forcing in this region.

The mean vertical and horizontal current structure affects the surface mean eddy kinetic energy (EKE) because current shears impact baroclinic and barotropic instability processes and resulting mesoscale activity. Maximum mesoscale activity is expected along mean current streamlines, which are largely aligned with wind curl isolines in the offshore region where the Sverdrup balance prevails (see Marchesiello et al., 2003, for the California current system and Penven et al., 2005, for the Peruvian system). In order to illustrate the impact of the downscaled wind product on the mesoscale variability pattern, the mean surface geostrophic EKE was calculated for the various simulations and compared to satellite estimations. Anomalies can either be relative to the mean seasonal cycle (non-seasonal anomalies) or to varying monthly mean (intraseasonal anomalies only). This separation allows differentiating the contribution of the dominant timescales of variability (denoted total-EKE and intraseasonal-EKE). For a quantitative comparison, the spatial pattern correlation between model and observed EKE have been computed and are presented in Table 2. The spatial pattern correlations were calculated over a sub-domain defined as "Chilean box" extending from 24°S to 36°S and from the coast to 85°W. We chose this region because its mesoscale activity is particularly sensitive to the coastal wind profile with a marked offshore EKE maximum. A cut-off value is applied (80 cm^2/s^2 for total-EKE and 20 cm^2/s^2 for intraseasonal-EKE) to focus on the area of high kinetic energy. As a consistency check, a "Peruvian box" ([7–13°S]; [coast–90°W]) and a "Large box" ([5–40°S]; [coast–90°W]) covering most of the Humboldt system have been computed (but not shown) and the results were found similar to the "Chilean box".

Fig. 5 displays the mean nonseasonal eddy kinetic energy (total-EKE) in the three simulations. In the control R-ERS simulation, the EKE pattern is realistic over most of the Peru–Chile region, with a spatial pattern correlation reaching 0.75 (Table 2, right panel) over the "Chilean box" (0.74 over the "Large box", not shown). Model EKE magnitude tends to be slightly larger than observed along the Peruvian coast (as found also by Capet et al. (2008)) and lower

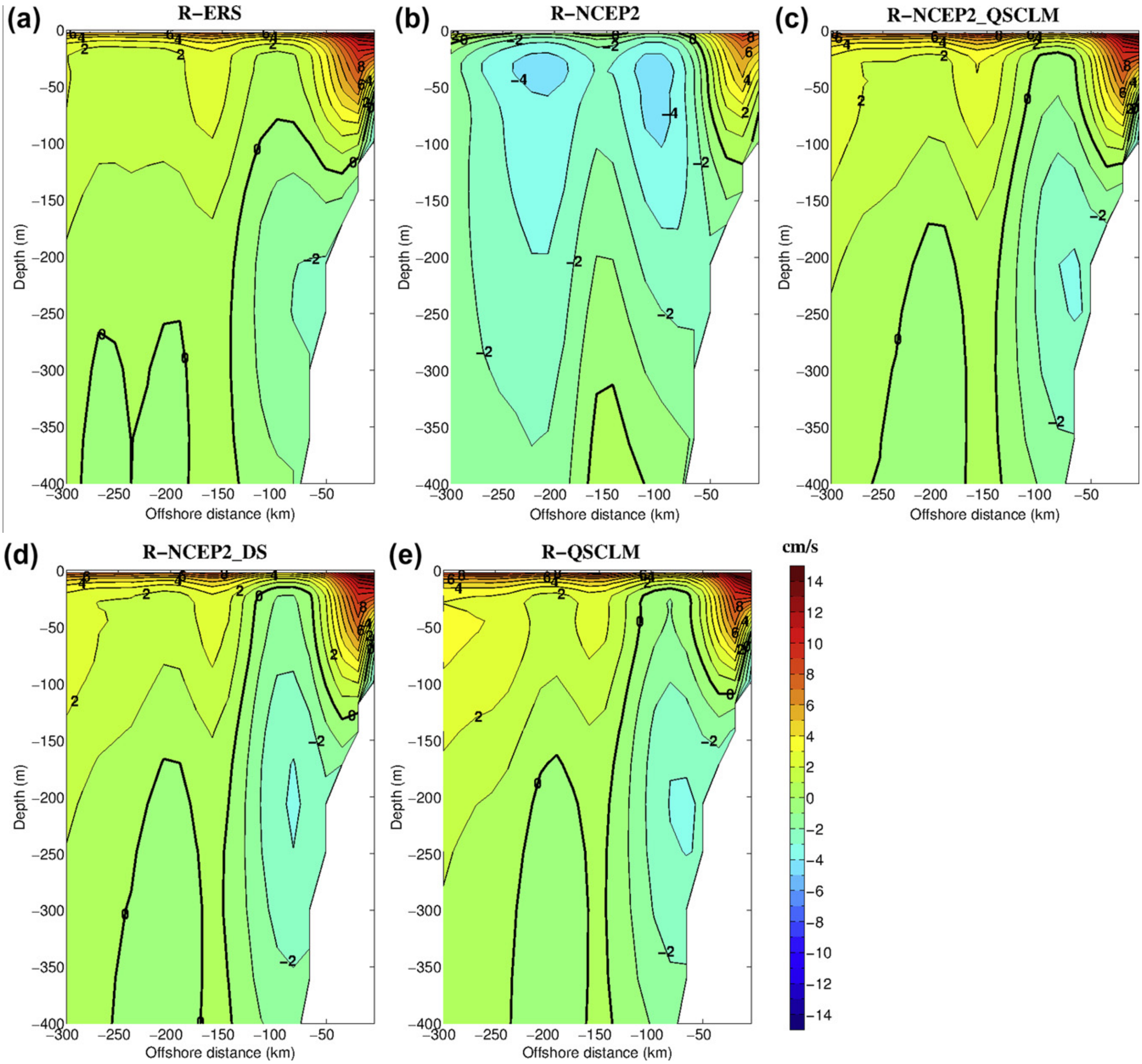

Fig. 4. Same as Fig. 3 but for the Central Chile region (alongshore-averaged between 30°S and 35°S).

along the Chilean coast. The AVISO product tends to underestimate EKE due to filtering procedures (e.g., comparisons with drifter estimations in Swenson and Niiler, 1996). Therefore, if mesoscale eddies are well resolved the model may outperform the satellite-based EKE estimation. Otherwise, the model EKE should be underestimated. Since the mesoscale energy injection scale is roughly given by the first baroclinic deformation wavelength, a 1/6° model resolution may thus be appropriate for the Peruvian region where the eddy scale is large, but less so in the Chilean region (see Penven et al., 2005, for a discussion on eddy scales along the Peru region; and also Belmadani et al., 2012). Consequently, the R-ERS simulation appears to provide a rational solution at the given resolution.

In the R-NCEP2 simulation, the EKE pattern is significantly degraded and the spatial pattern correlation with AVISO estimations is 0.6. EKE maxima are located too far offshore and have too broad an extent, consistent with SSH (and wind curl) pattern. R-NCEP2_QSCLM is able to correct most of the pattern bias found in R-NCEP2 (in SSH and EKE) and gives a very close solution to R-QSCLM. This result confirms that non-seasonal forcing have little effect on mean eddy energy with only a small part of EKE being associated with interannual forcing (differences are even smaller for intraseasonal-EKE; not shown). R-NCEP2_DS allows for a significant improvement of the simulated EKE. The correlations are higher with AVISO estimations and the patterns and amplitudes are much closer to R-ERS. This again suggests that the projection of NCEP2 low-frequency variability and trends on the downscaled wind product positively impacts both mean currents and eddies.

3.3. Intraseasonal variability

By construction, the downscaling method of Goubanova et al. (2011) is well suited to capture the variability that originates from the subtropical pressure system, with its strong intraseasonal variability. In order to estimate the extent to which R-NCEP2_DS can skillfully account for the intraseasonal variability of coastal circulation, the dominant mode of the meridional current for the intraseasonal frequency band (i.e. 5–70 $(\text{days})^{-1}$) is calculated for the

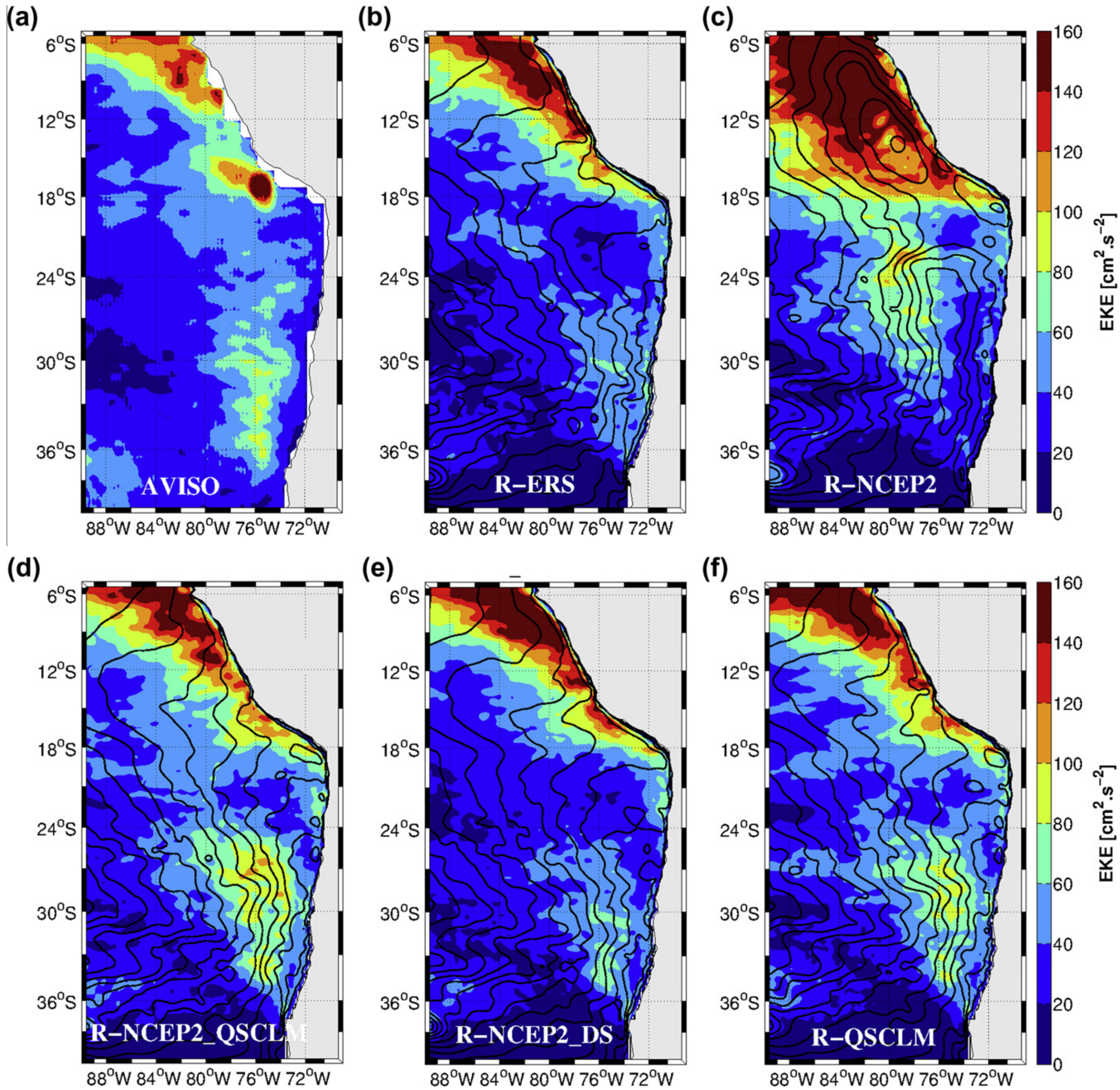

Fig. 5. Mean surface eddy kinetic energy (total-EKE, in $cm^2\ s^{-2}$) computed from sea level pressure gradients between 1992 and 2000 for (a) AVISO observations, (b) R-ERS, (c) R-NCEP2, (d) R-NCEP2_QSCLM, (e) R-NCEP2_DS and (f) R-QSCLM. Contours of model mean sea surface height are overlaid in black to indicate mean geostrophic surface currents.

various experiments and for the regions off Central Peru and Central Chile. The calculation is performed over a domain that encompasses the vertical structure variability of coastal circulation, i.e., from the surface to 500 m depth and from the coast to ~300 km offshore. Intraseasonal anomalies are defined again here as deviations from the monthly mean, which is equivalent to a high-pass filter with a cut-off period of 90 days (Dewitte et al., 2011). Since intraseasonal variability along the coast is associated to a large extent with the equatorial Kelvin wave, the EOF analysis will grasp a peak variability in the frequency band of the equatorial Kelvin wave forcing, that is at frequencies between 50 and 70 day^{-1} (Dewitte et al., 2008, 2011). Therefore, the differences between the various experiments are most likely representative of the higher frequency variability. The results of the EOF analysis for the experiment R-QSCLM will be used as a benchmark for the evaluation of the variability originating from the equator.

Fig. 6 presents the results for the Central Peru region. It illustrates a large diversity of the intraseasonal mode although the latter tends to peak near the PCUC core for all experiments. The differences between experiments can be further evidenced in the spectrum of the associated EOF time series. In particular for the experiments using direct NCEP2 forcing (RNCEP2 and R-NCEP2_QSCLM), there is a much larger energy at frequencies larger than 30 $days^{-1}$, than for the other experiments. The best agreement between modes is for R-ERS and R-NCEP2_DS_7D, which indicates that the downscaled winds are successful in grasping coastal intraseasonal variability and that high-frequency synoptic winds (at scales lower than the week) have a noticeable impact on the ocean circulation. The R-NCEP2_QSCLM mode has a pattern

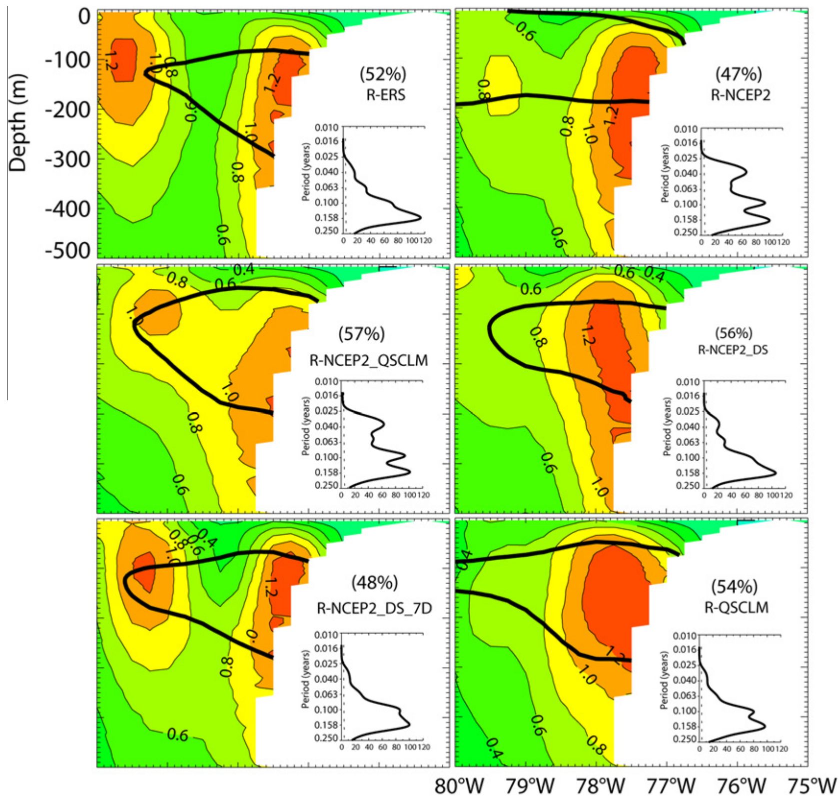

Fig. 6. First EOF of the vertical section of meridional current intraseasonal anomalies (in cm.s^{-1}) off Central Peru (alongshore-averaged between 7°S and 13°S) for the various simulations. The percentage of explained variance is indicated in each panel, together with time- and scale-averaged wavelet power spectrum of the associated time series (Torrence and Compo, 1998). The thick black line superimposed on the color plot is the 2 cm.s^{-1} isoline of the mean meridional current and indicates the core of the mean PCUC.

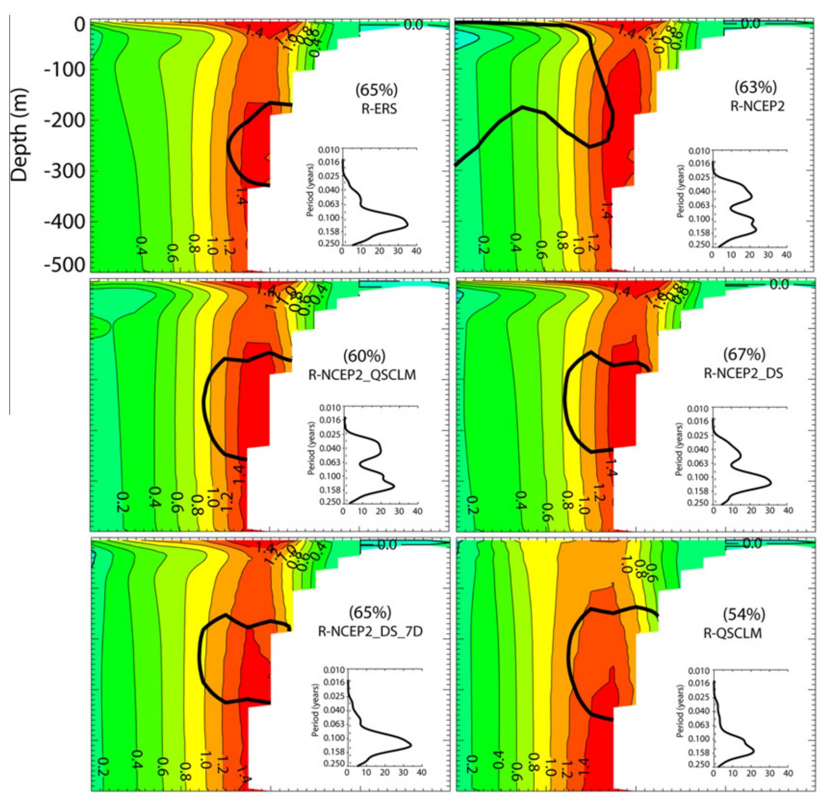

Fig. 7. Same as Fig. 6 but for the Central Chile region (meridional current intraseasonal anomalies are alongshore-averaged between 30°S and 35°S).

that extends too far offshore compared with R-ERS, similarly to R-QSCLM, indicating that the raw NCEP2 wind stress anomalies are not appropriate for a simulation of the PCUC intraseasonal variability.

Fig. 7 presents the comparison between experiments for the Central Chile region. It also indicates that R-NCEP2_DS_7D compares better with R-ERS than any other experiments both for the mode pattern and spectrum of its associated variability. Although all experiments tend to have an overall comparable intraseasonal mode pattern, the R-NCEP2 and R-NCEP2-QSCLM forcing have a much larger variability in the high-frequency band (in the range of periods between 5 and 30 days) than R-NCEP2_DS, which is not realistic as suggested by the results of R-ERS.

Summarizing, this analysis illustrates the good agreement of the intraseasonal mode between the two simulations R-ERS and R-NCEP2_DS (R-NCEP2_DS_7D) and highlights the efficiency of the downscaling method for simulating the oceanic intraseasonal variability off Central Peru and Central Chile.

3.4. Interannual variability

The potential of NCEP2_DS wind stress for long-term oceanic simulation needs to be evaluated with regards to its ability to account for the interannual variability, in particular the El Niño–La Niña conditions that are highly influential on the Peru and Chile current system. While off Peru the upwelling variability during El Niño is highly sensitive to the oceanic equatorial Kelvin wave (Colas et al., 2008) and to a lesser extend to the winds (Bakun and Weeks, 2008), off Central Chile, there is a weaker oceanic teleconnection but a marked atmospheric teleconnection that is influential on the upwelling with the winds decreasing during El Niño and increasing during La Niña (Montecinos and Gomez, 2010). Goubanova et al. (2011) showed that the statistical downscaling scheme allows capturing some of the interannual variability of upwelling-favorable winds, although with a reduced amplitude compared to observations (off Peru in particular). The mean conditions during the peak phases of El Niño (Dec 1997–Feb 1998) and

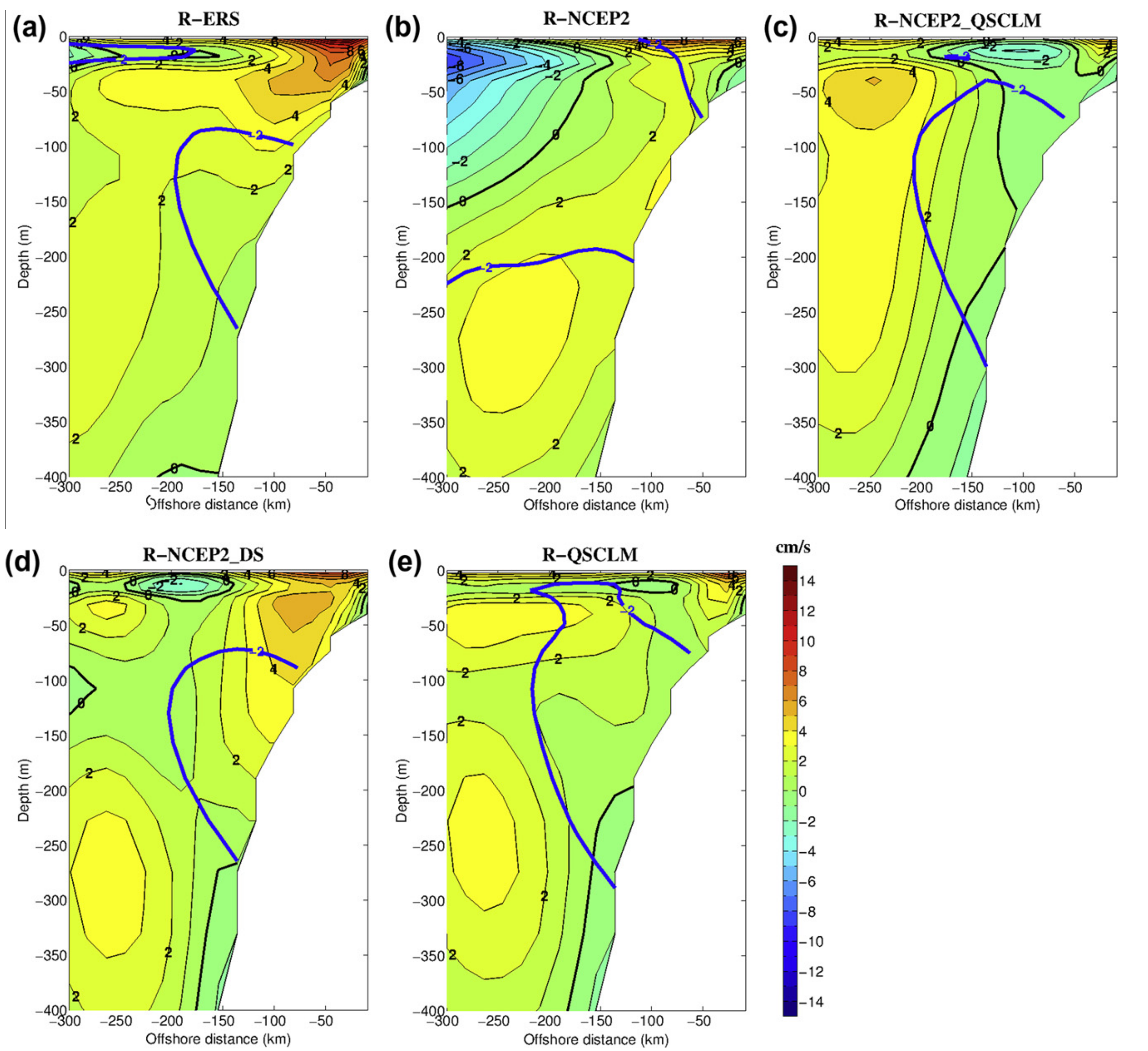

Fig. 8. Vertical sections of meridional current (in cm.s^{-1}) off Central Peru (alongshore-averaged between 7°S and 13°S) during the El Niño peak phases (December 97 to February 98) for the various simulations. Contour interval is 1 cm.s^{-1}. The thick blue line superimposed on the color plot is the 2 cm.s^{-1} isoline of mean meridional current and indicates the core of the mean PCUC.

La Niña (Dec 1998–Feb 1999) were computed off Central Peru and Central Chile (Figs. 8 and 9). The experiment R-ERS will be considered as a benchmark to evaluate the realism of interannual variability. It indicates that overall, during El Niño, the PCUC decreases (positive anomalies, relative to the mean state presented in Figs. 3 and 4) while it increases during La Niña (negative anomalies; not shown). During the El Niño peak phase off Peru (Fig. 8), the PCUC decreases and even disappears (compared with mean values in Fig. 3), essentially as a result of the downwelling oceanic Kelvin wave, whereas the surface northward current (averaged over the first 50–100 m) tends to extend further offshore. In comparison with the R-ERS control run, R-NECP2_DS clearly captures this pattern with much more realism than the other experiments. Similarly, during la Niña (not shown), the changes in the coastal currents are also better represented with intensified surface currents and a PCUC that is deeper and closer to the coast. The realism of R-NCEP2_DS is further illustrated off Central Chile in Fig. 9 (to be compared with Fig. 4), which shows that El Niño conditions are associated with a strong intensification and deepening of surface coastal currents flowing equatorward, around 100–150 km from the coast. As in the Peru region, the PCUC has weakened and the poleward subsurface PCCC (Strub et al, 1998) even more, with a reduction of its vertical extension from over 400 m in normal conditions to less than 150–200 m in El Niño conditions. These features are well simulated in R-NCEP2_DS as evidenced by the comparable location and strength of the core current between R-ERS and R-NCEP2_DS.

Finally, in order to provide a quantitative estimate of the impact of the downscaling method on the oceanic simulations presented in this paper, a validation from tide gauges observation is performed. We performed the analysis on 9 tide gauges stations (correlation and skill scores in Table 3), along the Peruvian and Chilean coast, from Talara (4.58°S) to Valparaiso (33.03°S). The simulation R-NCEP2_DS generally presents the best scores, particularly in the Peru region. It is always better than R-ERS except for Pisco and Matarani, and better than R-NCEP2 except off northern Chile (17°S and 23°S). Interestingly, R-NCEP2 presents the highest score in this region, suggesting the possibility of local deficiencies in the scatterometer data (Croquette et al., 2007). Overall, the gauge comparison confirms the improvements made by statistical

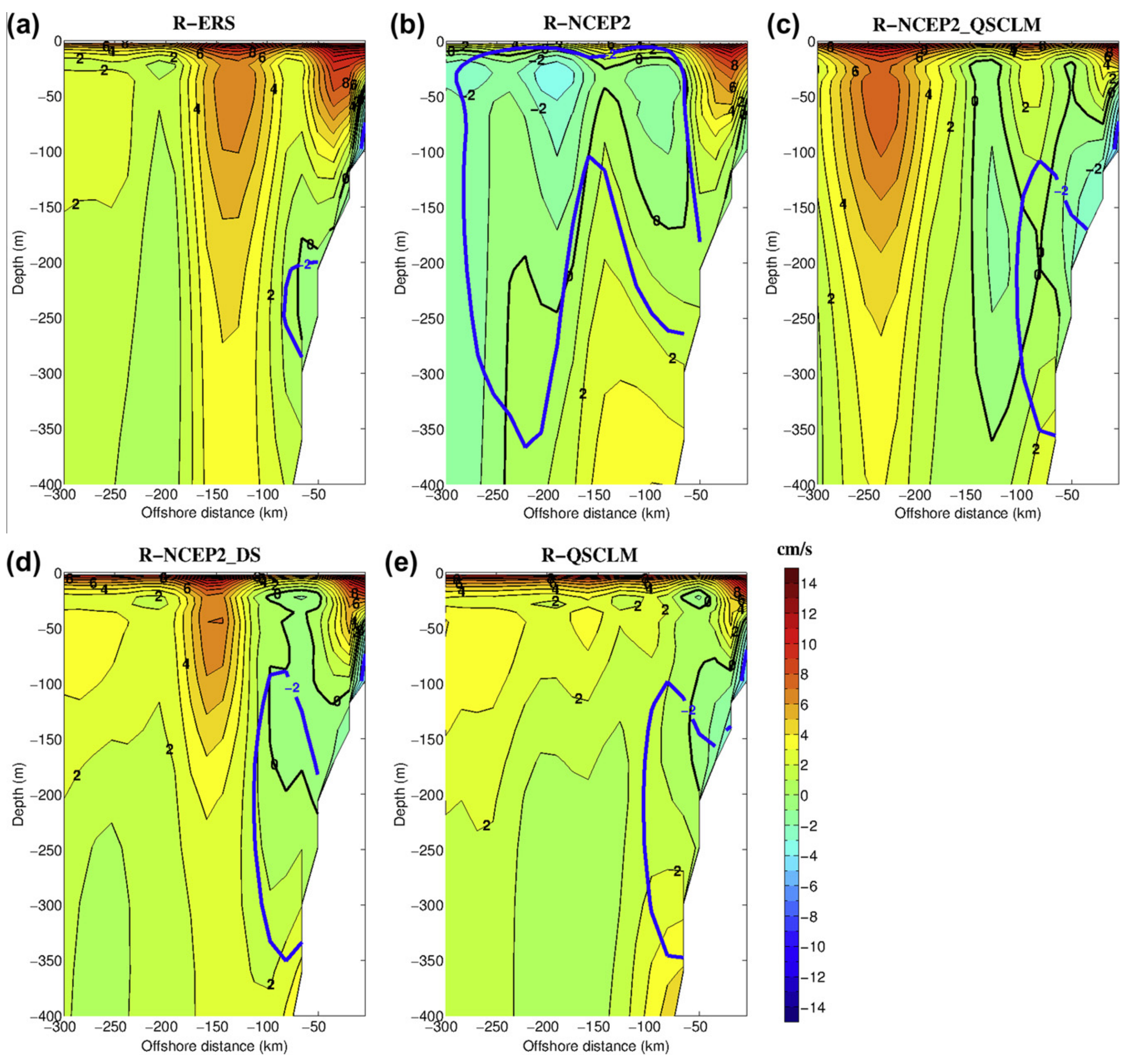

Fig. 9. Same as Fig. 8 but for the Central Chile region (alongshore-averaged between 30°S and 35°S).

downscaling of the NCEP2 product, at least over the 1992–2000 period. These results are also consistent with former modeling and observational studies (Pizarro et al., 2002; Colas et al., 2008) suggesting that interannual oceanic scales are sensitive to high resolution wind forcing.

4. Summary and conclusion

The issue of atmospheric forcing in ocean modeling of eastern boundary current systems is critical because of the sensitivity of upwelling dynamics to the structure and amplitude of coastal winds. Considering the current uncertainty in the evolution of upwelling ecosystems (Chavez et al., 2008), there is a stringent need for atmospheric forcing that can appropriately drive long-term, high-resolution oceanic simulations. Here, we evaluated the impact of downscaled winds derived from the NCEP2 reanalysis on the regional circulation off Peru and Chile over the 1992–2000 period, taking advantage of the availability of ERS winds for validation. The method for deriving the downscaled product is simple, cost effective and allows for reducing the major bias found in the reanalysis, i.e. the unrealistic coastal wind drop off and associated wind stress curl (Goubanova et al., 2011). It is shown that despite the deficiency of the statistical method for capturing the observed magnitude of the intraseasonal and interannual variability, its impact on the regional circulation is significant and allows for correcting major biases in the oceanic response to NCEP2. The mean and eddy circulation is already greatly improved by the use of mean seasonal QuikSCAT forcing. More interestingly perhaps, the intraseasonal and interannual variability also share more common characteristics with the control run (R-ERS) in the simulation forced by downscaled intraseasonal and interannual winds. Due to differences in satellite wind products (Croquette et al., 2007), the evaluation of the oceanic response to downscaled winds presents some limitation in the validation process. It was checked however (not shown) that a higher-resolution atmospheric reanalysis (the ERA-interim Reanalysis of the European center, 50 km resolution) and a dynamical downscaling product at medium resolution (WRF at 50 km resolution) do not improve the realism of our oceanic simulations. Our understanding is that both atmospheric products present deficiencies in reproducing the coastal wind profile. This is of course a superficial comparison of downscaling approaches; much effort is presently being devoted to producing high-resolution reanalysis from the dynamical downscaling approach (see CORDEX project[1]). Nevertheless, our results illustrate the proposition that statistical methods are a relevant alternative to costly simulations. We believe that the simple statistical method of Goubanova et al. (2011) can provide realistic forcing for long-term simulations that are needed for a better understanding of the variability and long-term trend of the Humboldt current system. Regional model studies dedicated to the climate change issue can also make use of this statistical approach. Echevin et al. (2012) provide a recent example for the Humboldt system. It will be extended to other upwelling systems and for long-term retrospective simulations.

Acknowledgments

We are grateful to B. Giese from Texas A&M University for providing the 5 day-mean outputs of SODA and to F. Colas for discussions. The two anonymous reviewers are also thanked for their constructive comments. The ROMS simulations were performed on a PC cluster supported by the IRD/DSF "Spirales" project and using HPC resources from CALMIP (Grant 2012-[1044]). K. Goubanova was supported by the ANR and AXA during the course of this study. This work was initiated and developed in the frame of the PCCC project and is a contribution to the PEPS ANR-08-VULN-12 project (ANR, France).

[1] CORDEX : COordinated Regional climate Downscaling Experiment http://wcrp.ipsl.jussieu.fr/SF_RCD_CORDEX.html.

References

Aguirre, C., Pizarro, O., Strub, T., Garreaud, R., Barth, J., 2012. Seasonal dynamics of the alongshore flow off Central Chile. J. Geophys. Res. Ocean 117, C01006. http://dx.doi.org/10.1029/2011JC007379.

Albert, A., Echevin, V., Lévy, M., Aumont, O., 2010. Impact of nearshore wind stress curl on coastal circulation and primary productivity in the Peru upwelling system. J. Geophys. Res. 115, C12033. http://dx.doi.org/10.1029/2010JC006569.

Barnier, B., Siefridt, L., Marchesiello, P., 1995. Thermal forcing for a global ocean circulation model using a three-year climatology of ECMWF analyses. J. Mar. Syst. 6, 363–380.

Bakun, Weeks, 2008. The marine ecosystem off Peru: what are the secrets of its fishery productivity and what might its future hold? Prog. Oceanogr. 79, 290–299.

Beckmann, A., Haidvogel, D.B., 1993. Numerical simulation of flow around a tall isolated seamount. Part I: Problem formulation and model accuracy. J. Phys. Oceanogr. 23, 1736–1753.

Belmadani, A., Echevin, V., Dewitte, B., Colas, F., 2012. Equatorially forced intraseasonal propagations along the Peru–Chile coast and their relation with the nearshore eddy activity in 1992–2000: a modelling study. J. Geophys. Res. Oceans 117, C04025, http://dx.doi.org/10.1029/2011JC007848.

Bentamy, A., Quilfen, Y., Gohin, F., Grima, N., Lenaour, M., Servain, J., 1996. Determination and validation of average wind fields from ERS-1 scatterometer measurements. Global Atmos. Ocean Syst. 4, 1–29.

Blanco, J.L., Thomas, A.C., Carr, M.-E., Strub, P.T., 2001. Seasonal climatology of hydrographic conditions in the upwelling region off northern Chile. J. Geophys. Res. 106, 11451–11467.

Capet, X., Marchesiello, P., McWilliams, J., 2004. Upwelling response to coastal wind profiles. Geophys. Res. Lett 31 (13), L13309. http://dx.doi.org/10.1029/2004GL020303.

Capet, X., Colas, F., Penven, P., Marchesiello, P., McWilliams, J.C., 2008. Eddies in eastern boundary subtropical upwelling systems. Eddy-Resolving Ocean Modeling, vol. 177. AGU Monograph, Washington DC, p. 350.

Carrère, L., Lyard, F., 2003. Modeling the barotropic response of the global ocean to atmospheric wind and pressure forcing? Comparison with observations. Geophys. Res. Lett. 30 (6), 1275.

Carr, M.-E., Kearns, E., 2003. Production regimes in four eastern boundary current systems. Deep Sea Res. II 50 (22–26), 3199–3221.

Carton, J.A., Giese, B.S., 2008. A reanalysis of ocean climate using Simple Ocean Data Assimilation (SODA). Mon. Weather Rev. 136, 2999–3017. http://dx.doi.org/10.1175/2007MWR1978.1.

CERSAT, 2002a. Mean wind fields (MWF product) user manual volume 1: ERS-1, ERS-2 & NSCAT. Rep C2-MUT-W-05-IF. CERSAT-IFREMER, Brest.

CERSAT, 2002b. Mean wind fields (MWF product) user manual volume 1: QuikSCAT. Rep C2-MUT-W-04-IF. CERSAT-IFREMER, Brest.

Chavez, F.P., Bertrand, A., Guevara-Carrasco, R., Soler, P., Csirke, J., 2008. The northern Humboldt current system: brief history, present status and a view towards the future. Prog. Oceanogr. 79, 95–105.

Chelton, D.B., Schlax, M.G., Samelson, R.M., 2007. Summertime coupling between sea surface temperature and wind stress in the California current system. J. Phys. Oceanogr. 37, 495–517.

Colas, F., Capet, X., McWilliams, J.C., Shchepetkin, A., 2008. 1997–98 El Niño off Peru: a numerical study. Prog. Oceanogr. 79, 138–155.

Colas, F., McWilliams, J.C., Capet, X., Kurian, J., 2011. Heat balance and eddies in the Peru–Chile current system. Clim. Dyn.. http://dx.doi.org/10.1007/s00382-011-1170-6.

Croquette, M., Eldin, G., Grados, C., Tamayo, M., 2007. On differences in satellite wind products and their effects in estimating coastal upwelling processes in the South–East Pacific. Geophys. Res. Lett. 34, l11608.

Da Silva, A.M., Young-Molling, C.C., Levitus, S. (Eds.), 1994. Atlas of Surface Marine Data 1994. Algorithms and Procedures, NOAA Atlas NESDIS, vol. 1. NOAA, Silver, Spring, MD, vol. 6, 83 pp.

Debreu, L., Marchesiello, P., Penven, P., Cambon, G., 2012. Two-way nesting in split-explicit ocean models: algorithms, implementation and validation. Ocean Modell. 49–50, 1–21.

Dewitte, B., Purca, S., Illig, S., Renault, L., Giese, B., 2008. Low frequency modulation of the intraseasonal equatorial Kelvin wave activity in the Pacific ocean from SODA: 1958–2001. J. Clim. 21, 6060–6069.

Dewitte, B., Illig, S., Renault, L., Goubanova, K., Takahashi, K., Gushchina, D., Mosquera, K., Purca, S., 2011. Modes of covariability between sea surface temperature and wind stress intraseasonal anomalies along the coast of Peru from satellite observations (2000–2008). J. Geophys. Res. 116, C04028. http://dx.doi.org/10.1029/2010JC006495.

Ducet, N., Le Traon, P.Y., Reverdin, G., 2000. Global high-resolution mapping of ocean circulation from TOPEX/Poseidon and ERS-1 and -2. J. Geophys. Res. 105 (C8), 19477–19498. http://dx.doi.org/10.1029/2000JC900063.

Echevin, V., Colas, F., Chaigneau, A., Penven, P., 2011. Sensitivity of the Northern Humboldt current system nearshore modeled circulation to initial and boundary conditions. J. Geophys. Res. 116, C07002. http://dx.doi.org/10.1029/2010JC006684.

Echevin, V., Goubanova, K., Belmadani, A., Dewitte, B., 2012. Sensitivity of the Humboldt current system to global warming: a downscaling experiment of the IPSL-CM4 model. Clim. Dyn.. http://dx.doi.org/10.1007/s00382-011-1085-2.

Estrade, P., Marchesiello, P., Colin de Verdiere, A., Roy, C., 2008. Cross-shelf structure of coastal upwelling: a two-dimensional expansion of Ekman's theory and a mechanism for innershelf upwelling shut down. J. Mar. Res. 66, 589–616.

Garreaud, R., Munoz, R., 2005. The low-level jet off the subtropical west coast of South America: structure and variability. Mon. Weather Rev. 133, 2246–2261.

Goubanova, K., Echevin, V., Dewitte, B., Codron, F., Takahashi, K., Terray, P., Vrac, M., 2011. Statistical downscaling of sea-surface wind over the Peru–Chile upwelling region: diagnosing the impact of climate change from the IPSL-CM4 model. Clim. Dyn. http://dx.doi.org/10.1007/s00382-010-0824-0.

Gruber, N., Lachkar, Z., Frenzel, H., Marchesiello, P., Munnich, M., McWilliams, J.C., Nagai, T., Plattner, G.-K., 2011. Mesoscale eddy-induced reduction in eastern boundary upwelling systems. Nat. Geosci. 4, 787–792.

Halpern, D., 2002. Offshore Ekman transport and Ekman pumping off Peru during the 1997–1998 El Niño. Geophys. Res. Lett. 29 (5), 1075. http://dx.doi.org/10.1029/2001GL014097.

Hormazabal, S., Shaffer, G., Letelier, J., Ulloa, O., 2001. Local and remote forcing of sea surface temperature in the coastal upwelling system off Chile. J. Geophys. Res. 106 (C8), 16657–16671.

Hormazabal, S., Shaffer, G., Pizarro, O., 2002. Tropical Pacific control of intraseasonal oscillations off Chile by way of oceanic and atmospheric pathways. Geophys. Res. Lett. 29. http://dx.doi.org/10.1029/2001GL013481.

Kanamitsu, M., Ebisuzaki, W., Woollen, J., Yang, S.-K., Hnilo, J.J., Fiorino, M., Potter, G.L., 2002 (NCEP-DEO AMIP-II reanalysis (R-2)). Bull. Atmos. Meteor. Soc., 1631–1643.

Large, W., McWilliams, J., Doney, S., 1994. Oceanic vertical mixing: a review and a model with a nonlocal boundary layer parameterization. Rev. Geophys. 32, 363–403.

Marchesiello, P., McWilliams, J.C., Shchepetkin, A., 2001. Open boundary conditions for long-term integration of regional oceanic models. Ocean Modell. 3, 1–20.

Marchesiello, P., McWilliams, J., Shchepetkin, A., 2003. Equilibrium structure and dynamics of the California current system. J. Phys. Oceanogr. 33, 753–783.

Marchesiello, P.L., Debreu, Couvelard, X., 2009 (Spurious diapycnal mixing in terrain-following coordinate models: the problem and a solution). Ocean Modell. 26, 156–169.

Marchesiello, P., Estrade, P., 2010. Upwelling limitation by onshore geostrophic flow. J. Mar. Res. 68, 37–62.

Montes, I., Colas, F., Capet, X., Schneider, W., 2010. On the pathways of the equatorial subsurface currents in the eastern equatorial Pacific and their contributions to the Peru–Chile undercurrent. J. Geophys. Res. 115, C09003. http://dx.doi.org/10.1029/2009JC005710.

Montes, I., Schneider, W., Colas, F., Blanke, B., Echevin, V., 2011. Subsurface connections in the eastern tropical Pacific during La Niña 1999–2001 and El Niño 2002–2003. J. Geophys. Res. 116, C12022. http://dx.doi.org/10.1029/2011JC007624.

Montecinos, Gomez, 2010. ENSO modulation of the upwelling season off southern-Central Chile. Geophys. Res. Lett. 33. http://dx.doi.org/10.1029/2009GL041739, L02708, 4 pp.

Muñoz, R., Garreaud, R., 2005. Dynamics of the low-level jet off the subtropical west coast of South America. Mon. Weather Rev. 133, 3661–3677.

Penven, P., Echevin, V., Pasapera, J., Colas, F., Tam, J., 2005. Average circulation, seasonal cycle, and mesoscale dynamics of the Peru current system: a modeling approach. J. Geophys. Res. 110, C10021. http://dx.doi.org/10.1029/2005JC002945.

Penven, P., Debreu, L., Marchesiello, P., McWilliams, J.C., 2006. Evaluation and application of the ROMS 1-way embedding procedure to the Central California upwelling system. Ocean Modell. 12, 157–187.

Penven, P., Marchesiello, P., Debreu, L., Lefevre, J., 2008. Software tools for pre- and post-processing of oceanic regional simulations. Environ. Model. Softw. 23, 660–662.

Pizarro, O., Shaffer, G., Dewitte, B., Ramos, M., 2002. Dynamics of seasonal and interannual variability of the Peru–Chile Undercurrent. Geophys. Res. Lett. 29 (12), 1581. http://dx.doi.org/10.1029/2002GL014790.

Ray, R.D., 1999. A global ocean tide model from TOPEX/Poseidon alrimetry: GOT4.7, NASA Tech. Memo. 209478, Goddard Space Flight Center, Greenbelt, 58 pp.

Renault, L., Dewitte, B., Falvey, M., Garreaud, R., Echevin, V., Bonjean, F., 2009. Impact of atmospheric coastal jets on SST off Central Chile from satellite observations (2000–2007). J. Geophys. Res. 114, C08006. http://dx.doi.org/10.1029/2008JC005083.

Renault, L., Dewitte, B., Marchesiello, P., Illig, S., Echevin, V., Cambon, G., Ramos, M., Astudillo, O., Minnis, P., Ayers, J.K., 2012. Upwelling response to atmospheric coastal jets off Central Chile: a modeling study of the October 2000 event. J. Geophys. Res. 117, C02030. http://dx.doi.org/10.1029/2011JC007446.

Reynolds, R.W., Smith, T.M., Liu, C., Chelton, D.B., Casey, K.S., Schlax, M.G., 2007. Daily high-resolution blended analyses for sea surface temperature. J. Clim. 20, 5473–5496.

Ridgway, K.R., Dunn, J.R., Wilkin, J.L., 2002. Ocean interpolation by four-dimension least-squares – application to the waters around Australia. J. Atmos. Oceanic Technol. 19 (9), 1357–1375. http://dx.doi.org/10.1175/1520.

Rouault, M., Penven, P., Pohl, B., 2009. Warming in the Agulhas current system since the 1980s. Geophys. Res. Lett. 36, L12602. http://dx.doi.org/10.1029/2009GL037987.

Shaffer, G., Hormazabal, S., Pizarro, O., Salinas, S., 1999. Seasonal and interannual variability of currents and temperature off Central Chile. J. Geophys. Res. 104, 29951–29961.

Shchepetkin, A.F., McWilliams, J.C., 2005. The Regional oceanic modeling system: a split-explicit, free-surface, topography following – coordinate ocean model. Ocean Modell. 9, 347–404. http://dx.doi.org/10.1016/j.ocemod.2004.08.002.

Smith, R., Dukowicz, J.K., Malone, R.C., 1992. Parallel ocean general circulation modelling. Phys. D 60, 38–61.

Smith, W.H.F., Sandwell, D.T., 1997. Global seafloor topography from satellite altimetry and ship depth soundings. Science 277, 1957–1962.

Strub, P.T., Mesias, J.M., Montecino, V., Ruttlant, J., Salinas, S., 1998 (The sea). Coastal Ocean Circulation Off Western South America, vol. 11. Wiley, London, Chap. 10, pp. 29–67.

Swenson, M.S., Niiler, P.P., 1996. Statistical analysis of the surface circulation of the California current. J. Geophys. Res. 101 (C10), 22631–22645.

Taylor, K.E., 2001. Summarizing multiple aspects of model performance in a single diagram. J. Geophys. Res. 106 (D7), 7183–7192. http://dx.doi.org/10.1029/2000JD900719.

Torrence, C., Compo, G.P., 1998. A practical guide to wavelet analysis. Bull. Am. Meteor. Soc. 79, 61–78, http://dx.doi.org/10.1175/1520-0477(1998)079<0061:APGTWA>2.0.CO;2.

Tulloch, R., Marshall, J., Hill, C., Smith, K.S., 2011. Scales, growth rates and spectral fluxes of baroclinic instability in the ocean. J. Phys. Oceanogr., 1057–1076.